Article

High-order harmonic source spanning up to the oxygen K-edge based on filamentation pulse compression

SCHMIDT, Cédric, *et al*.

Abstract

We present a 0.2 TW sub-two-cycle 1.8 μm carrier-envelope-phase stable source based on two-stage pulse compression by filamentation for driving high-order harmonic generation extending beyond the oxygen K absorption edge. The 1 kHz repetition rate, high temporal resolution enabled by the short 11.8 fs driving pulse duration, and bright high-order harmonics generated in helium make this an attractive source for solid-state and molecular-dynamics studies.

Reference

SCHMIDT, Cédric, *et al*. High-order harmonic source spanning up to the oxygen K-edge based on filamentation pulse compression. *Optics Express*, 2018, vol. 26, no. 9, p. 11834

DOI : 10.1364/OE.26.011834

Research Article | Vol. 26, No. 9 | 30 Apr 2018 | OPTICS EXPRESS 11834
Optics EXPRESS

High-order harmonic source spanning up to the oxygen K-edge based on filamentation pulse compression

CÉDRIC SCHMIDT,[1] YOANN PERTOT,[2] TADAS BALCIUNAS,[1] KRISTINA ZINCHENKO,[2] MARY MATTHEWS,[1] HANS JAKOB WÖRNER,[2] AND JEAN-PIERRE WOLF[1,*]

[1]*Department of Applied Physics, University of Geneva, 1227 Carouge, Switzerland*
[2]*Laboratory of Physical Chemistry, ETH Zurich, 8093 Zurich, Switzerland*
[*]*jean-pierre.wolf@unige.ch*
http://www.unige.ch/gap/biophotonics

Abstract: We present a 0.2 TW sub-two-cycle 1.8 μm carrier-envelope-phase stable source based on two-stage pulse compression by filamentation for driving high-order harmonic generation extending beyond the oxygen K absorption edge. The 1 kHz repetition rate, high temporal resolution enabled by the short 11.8 fs driving pulse duration and bright high-order harmonics generated in helium make this an attractive source for solid-state and molecular-dynamics studies.

OCIS codes: (320.0320) Ultrafast optics; (320.5520) Pulse compression; (020.2649) Strong field laser physics.

References and links

1. E. Goulielmakis, Z.-H. Loh, A. Wirth, R. Santra, N. Rohringer, V. S. Yakovlev, S. Zherebtsov, T. Pfeifer, A. M. Azzeer, M. F. Kling, S. R. Leone, and F. Krausz, "Real-time observation of valence electron motion," Nature **466**, 739–743 (2010).
2. M. Holler, F. Schapper, L. Gallmann, and U. Keller, "Attosecond electron wave-packet interference observed by transient absorption," Phys. Rev. Lett. **106**, 123601 (2011).
3. M. Schultze, K. Ramasesha, C. Pemmaraju, S. Sato, D. Whitmore, A. Gandman, J. S. Prell, L. J. Borja, D. Prendergast, K. Yabana, D. M. Neumark, and S. R. Leone, "Attosecond band-gap dynamics in silicon," Science **346**, 1348–1352 (2014).
4. I. Jordan, M. Huppert, M. A. Brown, J. A. van Bokhoven, and H. J. Wörner, "Photoelectron spectrometer for attosecond spectroscopy of liquids and gases," Rev. Sci. Instruments **86**, 123905 (2015).
5. T. Popmintchev, M.-C. Chen, A. Bahabad, M. Gerrity, P. Sidorenko, O. Cohen, I. P. Christov, M. M. Murnane, and H. C. Kapteyn, "Phase matching of high harmonic generation in the soft and hard X-ray regions of the spectrum," Proc. Natl. Acad. Sci. **106**, 10516–10521 (2009).
6. T. Popmintchev, M.-C. Chen, D. Popmintchev, P. Arpin, S. Brown, S. Ališauskas, G. Andriukaitis, T. Balčiunas, O. D. Mücke, A. Pugzlys, A. Baltuška, B. Shim, S. E. Schrauth, A. Gaeta, C. Hernández-García, L. Plaja, A. Becker, A. Jaron-Becker, M. M. Murnane, and H. C. Kapteyn, "Bright coherent ultrahigh harmonics in the kev x-ray regime from mid-infrared femtosecond lasers," Science **336**, 1287–1291 (2012).
7. J. L. Krause, K. J. Schafer, and K. C. Kulander, "High-order harmonic generation from atoms and ions in the high intensity regime," Phys. Rev. Lett. **68**, 3535–3538 (1992).
8. J. Tate, T. Auguste, H. G. Muller, P. Salières, P. Agostini, and L. F. DiMauro, "Scaling of wave-packet dynamics in an intense midinfrared field," Phys. Rev. Lett. **98**, 013901 (2007).
9. S. Driever, D. Bigourd, N. Fedorov, M. Cornet, M. Arnold, F. Burgy, S. Montant, S. Petit, D. Descamps, E. Cormier, E. Constant, and A. Zair, "Tunable 1.6-2 um near infrared few-cycle pulse generation by filamentation," Appl. Phys. Lett. **102**, 191119 (2013).
10. Y. Pertot, C. Schmidt, M. Matthews, A. Chauvet, M. Huppert, V. Svoboda, A. von Conta, A. Tehlar, D. Baykusheva, J.-P. Wolf, and H. J. Wörner, "Time-resolved X-ray absorption spectroscopy with a water window high-harmonic source," Science **355**, 264–267 (2017).
11. N. Saito, N. Ishii, T. Kanai, S. Watanabe, and J. Itatani, "Attosecond streaking measurement of extreme ultraviolet pulses using a long-wavelength electric field," Sci. Reports **6**, 35594 (2016).
12. S. L. Cousin, N. Di Palo, B. Buades, S. M. Teichmann, M. Reduzzi, M. Devetta, A. Kheifets, G. Sansone, and J. Biegert, "Attosecond streaking in the water window: A new regime of attosecond pulse characterization," Phys. Rev. X **7**, 041030 (2017).
13. J. Li, X. Ren, Y. Yin, K. Zhao, A. Chew, Y. Cheng, E. Cunningham, Y. Wang, S. Hu, Y. Wu, M. Chini, and Z. Chang, "53-attosecond X-ray pulses reach the carbon k-edge," Nat. Commun. **8**, 186 (2017).

#320087 https://doi.org/10.1364/OE.26.011834
Journal © 2018 Received 18 Jan 2018; revised 28 Mar 2018; accepted 29 Mar 2018; published 24 Apr 2018

14. T. Gaumnitz, A. Jain, Y. Pertot, M. Huppert, I. Jordan, F. Ardana-Lamas, and H. J. Wörner, "Streaking of 43-attosecond soft-X-ray pulses generated by a passively CEP-stable mid-infrared driver," Opt. Express **25**, 27506–27518 (2017).
15. A. Couairon and A. Mysyrowicz, "Femtosecond filamentation in transparent media," Phys. Reports **441**, 47 – 189 (2007).
16. L. Bergé, S. Skupin, R. Nuter, J. Kasparian, and J.-P. Wolf, "Ultrashort filaments of light in weakly ionized, optically transparent media," Reports on Prog. Phys. **70**, 1633 (2007).
17. P. Béjot, E. Hertz, J. Kasparian, B. Lavorel, J. P. Wolf, and O. Faucher, "Transition from plasma-driven to kerr-driven laser filamentation," Phys. Rev. Lett. **106**, 243902 (2011).
18. N. Ishii, K. Kaneshima, K. Kitano, T. Kanai, S. Watanabe, and J. Itatani, "Carrier-envelope phase-dependent high harmonic generation in the water window using few-cycle infrared pulses," Nat. communications **5**, 4331 (2014).
19. V. Gruson, G. Ernotte, P. Lassonde, A. Laramée, M. R. Bionta, M. Chaker, L. Di Mauro, P. B. Corkum, H. Ibrahim, B. Schmidt, and F. Legaré, "2.5 TW, two-cycle IR laser pulses via frequency domain optical parametric amplification," Opt. Express **25**, 27706–27714 (2017).
20. H. J. Wörner, C. A. Arrell, N. Banerji, A. Cannizzo, M. Chergui, A. K. Das, P. Hamm, U. Keller, P. M. Kraus, E. Liberatore, P. Lopez-Tarifa, M. Lucchini, M. Meuwly, C. Milne, J.-E. Moser, U. Rothlisberger, G. Smolentsev, J. Teuscher, J. A. van Bokhoven, and O. Wenger, "Charge migration and charge transfer in molecular systems," Struct. Dyn. **4**, 061508 (2017).
21. S. Zahedpour, J. K. Wahlstrand, and H. M. Milchberg, "Measurement of the nonlinear refractive index of air constituents at mid-infrared wavelengths," Opt. Lett. **40**, 5794–5797 (2015).
22. B. E. Schmidt, P. Béjot, M. Giguère, A. D. Shiner, C. Trallero-Herrero, É. Bisson, J. Kasparian, J.-P. Wolf, D. M. Villeneuve, J.-C. Kieffer, P. B. Corkum, and F. Légaré, "Compression of 1.8 μm laser pulses to sub two optical cycles with bulk material," Appl. Phys. Lett. **96**, 121109 (2010).
23. P. Béjot, B. E. Schmidt, J. Kasparian, J.-P. Wolf, and F. Legaré, "Mechanism of hollow-core-fiber infrared-supercontinuum compression with bulk material," Phys. Rev. A **81**, 063828 (2010).
24. F. Silva, S. M. Teichmann, S. L. Cousin, M. Hemmer, and J. Biegert, "Spatiotemporal isolation of attosecond soft X-ray pulses in the water window," Nat. communications **6**, 6611 (2015).
25. S. L. Cousin, F. Silva, S. Teichmann, M. Hemmer, B. Buades, and J. Biegert, "High-flux table-top soft X-ray source driven by sub-2-cycle, CEP stable, 1.85-μm 1-kHz pulses for carbon K-edge spectroscopy," Opt. Lett. **39**, 5383–5386 (2014).
26. C. P. Hauri, W. Kornelis, F. W. Helbing, A. Heinrich, A. Couairon, A. Mysyrowicz, J. Biegert, and U. Keller, "Generation of intense, carrier-envelope phase-locked few-cycle laser pulses through filamentation," Applied Physics B - Laser and Optics. **79**, 673–677 (2004).
27. P. Panagiotopoulos, P. Whalen, M. Kolesik, and J. V. Moloney, "Super high power mid-infrared femtosecond light bullet," Nat. Photonics **9**, 543 (2015).
28. G. Agrawal, *Nonlinear Fiber Optics*, Optics and Photonics (Elsevier Science, 2001).
29. I. Ahmad, L. Bergé, Z. Major, F. Krausz, S. Karsch, and S. A. Trushin, "Redshift of few-cycle infrared pulses in the filamentation regime," New J. Phys. **13**, 093005 (2011).
30. C. Milián, V. Jukna, A. Couairon, A. Houard, B. Forestier, J. Carbonnel, Y. Liu, B. Prade, and A. Mysyrowicz, "Laser beam self-symmetrization in air in the multifilamentation regime," J. Phys. B: At. Mol. Opt. Phys. **48**, 094013 (2015).
31. B. Prade, M. Franco, A. Mysyrowicz, A. Couairon, H. Buersing, B. Eberle, M. Krenz, D. Seiffer, and O. Vasseur, "Spatial mode cleaning by femtosecond filamentation in air," Opt. Lett. **31**, 2601–2603 (2006).
32. W. Liu and S. L. Chin, "Abnormal wavelength dependence of the self-cleaning phenomenon during femtosecond-laser-pulse filamentation," Phys. Rev. A **76**, 013826 (2007).
33. G. Sansone, E. Benedetti, F. Calegari, C. Vozzi, L. Avaldi, R. Flammini, L. Poletto, P. Villoresi, C. Altucci, R. Velotta, S. Stagira, S. De Silvestri, and M. Nisoli, "Isolated single-cycle attosecond pulses," Science **314**, 443–446 (2006).
34. A. Baltuška, M. Uiberacker, E. Goulielmakis, R. Kienberger, V. S. Yakovlev, T. Udem, T. W. Hänsch, and F. Krausz, "Phase-Controlled Amplification of Few-Cycle Laser Pulses," IEEE Jnl. on Sel. Top. Quant. Elect. **9**, 972–989 (2003).
35. S. M. Teichmann, F. Silva, S. L. Cousin, M. Hemmer, and J. Biegert, "0.5-KeV soft X-ray attosecond continua," Nat. Commun. **7**, 11493 (2016).
36. C. P. Hauri, R. B. Lopez-Martens, C. I. Blaga, K. D. Schultz, J. Cryan, R. Chirla, P. Colosimo, G. Doumy, A. M. March, C. Roedig, E. Sistrunk, J. Tate, J. Wheeler, L. F. DiMauro, and E. P. Power, "Intense self-compressed, self-phase-stabilized few-cycle pulses at 2 from an optical filament," Opt. Lett. **32**, 868–870 (2007).

1. Introduction

High-order harmonic generation (HHG) based sources have recently achieved unprecedented, sub-femtosecond, temporal resolution in transient absorption measurements [1–3]. While the pioneering HHG experiments were performed using near-IR laser-based sources with a cut-off limited to the sub-100 eV range, most spectroscopic studies providing both attosecond time resolution and atomic spatial resolution require core electron excitation at significantly higher energies. In particular, the dynamics of organic and biological molecules would be optimally

Optics EXPRESS

addressed in the so-called water transparency window, which lies between the carbon and oxygen K-shell absorption edges (commonly 284-543 eV) enabling X-ray absorption measurements of aqueous solutions [4]. A well established technique to extend the HHG cut-off is to use longer wavelength (λ) driving pulses [5, 6], taking advantage of the well known λ^2 dependence of the cut off frequency [7]: $E_{max} \leqslant I_p + 3.17U_p$, where $U_p \propto \lambda^2 \cdot I_{\mathrm{L}}$ being the mean quiver energy of the electron in the laser field, I_{p} is the ionization potential of the generation medium and I_{L} is the intensity of the driving laser. The challenge of long-wavelength HHG driving is the drastically reduced single-atom yield which scales as $\lambda^{-5.5}$ [8, 9]. However, this partially can be compensated using favorable phase-matching conditions and increased medium density [6]. The short few-cycle duration driving pulses are highly desirable and allow HHG in the loose-focusing geometry thus increasing efficiency and compensating for the single-atom yield decrease.

The recent advancements in high power laser/parametric sources have achieved sufficient photon flux (kHz repetition rates) for performing time-resolved transient absorption measurements in the water window range [10] and techniques, such as attosecond streaking [11–13], have recently been extended to this spectral range enabling the generation of the shortest attosecond pulses ever produced [14].

In this paper we present a soft X-ray source extending well beyond the oxygen K-edge and reaching 570 eV, which is driven by sub-two-cycle 1.8 μm mid-IR pulses. The pulses are generated in an optical parametric amplifier (OPA) and post-compressed in two filamentation stages. Long wavelength driving pulses are attractive for pulse post-compression in a filament, as the critical power P_c scales with λ^2 [15,16]: $P_c \sim 3.72\lambda^2/(8\pi \cdot n_0 \cdot n_2)$, where n_0 and n_2 are the linear and Kerr refractive indices. Laser filaments are self-sustained light structures of 0.1 to 1 mm in diameter, spanning over hundreds of meters in length and producing a low-density plasma ($10^{15} - 10^{17}$ cm^{-3}) along their path. They stem from the dynamic balance between Kerr self-focusing and defocusing from the self-generated plasma and/or non-linear polarization saturation [17]. As the wavelength increases, the plasma density decreases and its role in counter-balancing the Kerr self-focusing decreases accordingly. The long wavelength driving pulses used in our scheme allow efficient and scalable filament-based pulse compression as discussed in Section 3 without the detrimental effects of plasma formation.

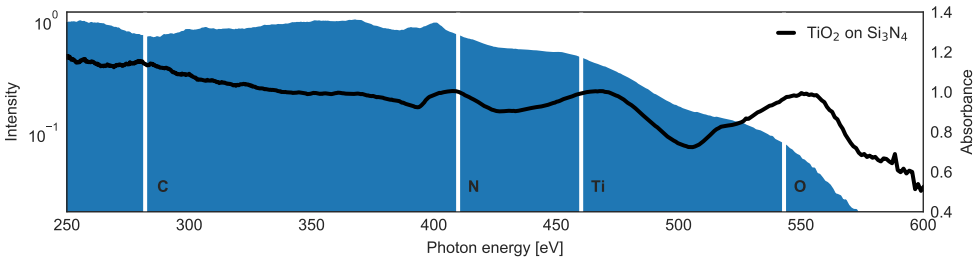

Fig. 1. Typical soft X-ray high harmonic spectrum covering the full water window. The generation is achieved in a gas target with over 2 bar of helium pressure. This spectrum is averaged over 30 acquisitions of 250 ms each. The black curve corresponds to the absorption spectrum of TiO_2 nanoparticles deposited on a Si_3N_4 substrate. The white lines indicate the energies of the carbon (C) K-edge at 282 eV, the nitrogen (N) K-edge at 410 eV, the titanium (Ti) L_2-edge at 460 eV and the oxygen (O) K-edge at 543 eV.

While broadband optical parametric chirped-pulse amplifiers based on BiBO nonlinear crystals [18] or parametric amplification in the Fourier-plane [19] have been previously successfully demonstrated, here we show that high flux HHG can be achieved using a much simpler and robust pulse compression method and a conventional BBO based Type-II optical parametric amplifier.

Optics EXPRESS

As compared to the first demonstration of the soft X-ray transient absorption measurements [10], here we extended the HHG spectrum to the 570 eV cut-off to cover the full water window. Bright X-ray supercontinuum covering the carbon, nitrogen and oxygen K-edges all together provides new perspectives for the investigation of charge-transfer dynamics in solids, nanoparticles, and liquids [20]. This was made possible by the improved pulse compression described later in this paper and by the use of helium, a higher I_p gas target as compared to neon. In addition to the extended cut-off, the shorter driving pulses provide higher temporal resolution in pump-probe experiments (as e.g. transient absorption).

2. Soft X-ray transient absorption setup

The experimental setup is summarized in Fig. 2. The commercial laser amplifier consists of a regenerative amplifier from Coherent delivering 4 mJ pulses that are subsequently amplified in a cryogenically-cooled two-pass amplifier (Coherent). The two-stage Ti:Sapphire based laser amplifier delivers 17 mJ 40 fs pulses at 1 kHz repetition rate. Most of the laser output of around 15 mJ is used to pump a BBO-based Type-II parametric amplifier (HE-TOPAS) from Light Conversion seeded with a white-light supercontinuum derived from the same pump pulse. The parametric amplifier delivers 2.5 mJ 40 fs idler pulses centered at $\lambda = 1.8\,\mu$m wavelength that are passively carrier-envelope-phase stabilized. This mid-IR output is then compressed down to sub-two cycles pulses in a dual stage filamentation arrangement, the optimization of which is described in detail in the next section.

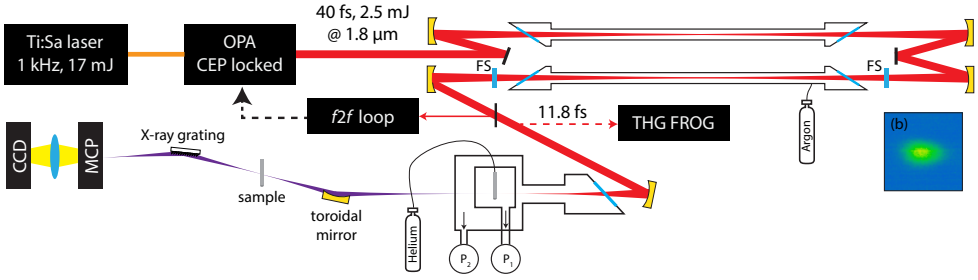

Fig. 2. Experimental layout with Ti:Sa amplified 800 nm pulse (in red) pumping the OPA with 15 mJ. The CEP stable 1.8 μm idler pulses (in yellow) are broadened by two successive filament lines of 4 m each and compressed in a fused silica plate of appropriate thickness. The compressed 11.8 fs pulse is focused into a high pressure helium target and drives the HHG process. Bottom: Detailed view of the high pressure target and the HHG scheme. P_1, P_2 and are the pressures measured in each of the differential pumping stages. Inset (b): the beam intensity profile of the focused post-compressed beam.

The water-window-spanning X-ray spectrum is generated by focusing the post-compressed pulses using a 350 mm focal length spherical mirror into a static high pressure helium gas target. The generation medium length in a laser-drilled tube target is 6 mm as depicted in Fig. 2. Typical backing pressure used for the HHG in helium is ≈ 2500 mbar. Using a three-stage differential pumping vacuum system, the pressure is reduced down to 10^{-6} mbar in the spectrometer chamber, necessary for the operation of the multi-channel-plate detector (MCP). The phase-matching conditions for the high-harmonic generation are optimized by controlling the gas pressure, target position and by fine-tuning the 1.8 μm driving pulse compression. The HHG radiation is filtered from the infrared pulses using a pinhole of 2 mm diameter and a 100 nm thick silver filter. The soft X-ray beam is then refocused with a nickel-coated grazing-incidence toroidal mirror onto the sample. In addition, a pump pulse is eventually recombined with the soft X-ray probe pulse

Optics EXPRESS

using an annular 45^o mirror. Finally, the transmitted probe pulse is analyzed in a flat-field X-ray spectrometer, which is based on a laminar-type replica 2400 groove/mm diffraction grating (Shimadzu) and a 40 mm diameter active area MCP imaging detector. The diffraction-limited (theoretical) resolution of the spectrometer is around 1 eV in the 300 eV spectral range. However, in order to reduce thermal load on the solid-state samples (TiO_2 nanoparticles), the spectrometer entrance slit was opened to shorten the integration time thus effectively reducing the spectral resolution.

The acquired X-ray spectrum shown in Fig. 1 (shaded curve) is calibrated in energy and sensitivity. The spectral calibration is based on the carbon K-edge absorption at 282 eV and static absorption lines observed in TiO_2 nanoparticles deposited on a Si_3N_4 substrate of 50 nm thickness. The intensity is then corrected with the grating efficiency curve provided by Shimadzu.

The static absorption spectrum of TiO_2, shown in Fig. 1 (black line) is obtained by comparing the transmitted X-ray spectrum with a reference one $A = -log_{10}(S/S_{ref})$. Both spectra are acquired keeping the same exposure parameters.

In optimal conditions of CEP stability, the harmonic cutoff energy is measured higher than the oxygen K-edge at 543 eV, meaning a full coverage of the so-called water window. The overall stability combined to the kHz pulse repetition rate allows a strong reduction of the acquisition time: for instance the spectrum presented in Fig. 1 is averaged over only 30 captures of 250 ms acquisition time each. First dynamic scans in experimental conditions similar to [10] allow to estimate a required time of less than 30 minutes for full transient absorption time-scans with femtosecond resolution. Although a precise and robust photon flux estimation of HHG sources is challenging as it requires taking into account spectral sensitivity of the detector, transmission of the refocusing optics, diffraction grating efficiency, we did a comparative flux calibration using a calibrated photodiode while keeping experimental conditions as similar as possible. We estimated the energy of the generated HHG radiation in the water window of around 2 pJ per laser pulse.

3. Sub-two cycle pulse compression

The 40-fs pulses centered at 1.8 μm from the parametric amplifier are post-compressed by spectral broadening in a two-stage filamentation stages. The usual break-up in multiple filaments, which occurs for laser powers P of the order of $10 \cdot P_c$ and limits the maximum energy in filament-based compression schemes, is therefore increased in the mid-IR. Moving from 800 nm to 1.8 μm provides thus roughly a factor 5 in energy before modulational instability induced break-up (n_2 assumed constant as reported in [21]) allowing single filaments bearing several mJ in few-cycles duration. In our case, the peak power after filamentation reaches 0.2 TW.

In comparison with hollow-core capillary-based pulse compression schemes [22–25], the filament-based pulse compression scheme introduces virtually no losses ($< 1\,\%$ measured at 2 bar of argon pressure, see Figs. 3(c) and 3(d)). Due to the absence of waveguide in our pulse post-compression scheme, the alignment is greatly simplified, and the pointing instabilities, and optical damage probability are also significantly reduced. In addition, operating in the infrared ($\lambda > 1.4$ μm) spectral range allows simple compensation of the induced chirp due to self-phase modulation (SPM) by the anomalous dispersion of common optical materials, such as fused silica or CaF_2.

The spectrum of the 1.8 μm idler pulses is broadened by loosely focussing using a 2 meter focal length spherical mirror in a first 3.5 meter long argon gas cell isolated by two 3-mm-thick CaF_2 windows cut at Brewster's angle for the first stage of spectral broadening. Using long focal length mirrors is crucial to reduce plasma formation and its associated losses and instabilities. The beam is then collimated using the same 2 meter focal length silver mirror and the residual chirp is compensated in a 2 mm thick fused silica glass plate and temporally compressing the pulse for further broadening. The pulse after the first compression stage is then launched into a second pulse compression stage consisting of an identical argon-filled cell for subsequent spectral broadening

Optics EXPRESS

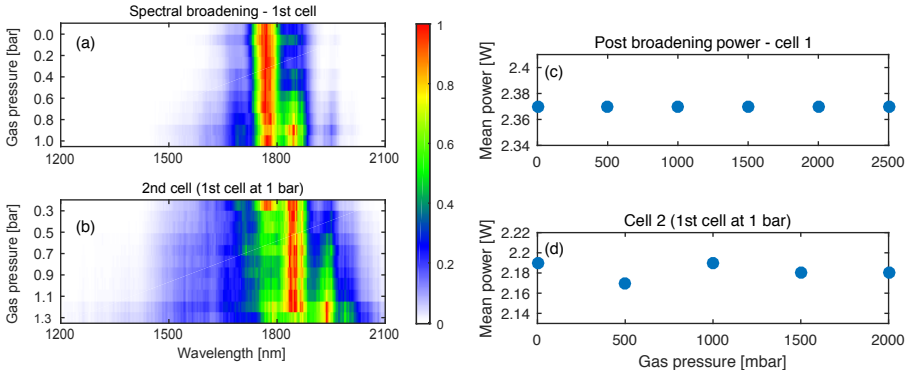

Fig. 3. Evolution of the pulse spectral broadening with increasing pressure in the first (a) and second gas cell (b) for the two-stage filament compression. For the second stage broadening (bottom), the pressure in the first cell is fixed at 1 bar. (c) Output pulse average power measurement at the output of each filament cell as a function of argon pressure in the (c) first gas cell and (d) second gas cell.

by filamentation. The gas pressure in each cell can be independently controlled ranging from vacuum to 3 bar of absolute pressure. The two-stage pulse compression arrangement allows achieving higher compression ratio and cleaner compressed pulses, as originally demonstrated by Hauri et al. [26] with a Ti:Sa laser [36] . The beam is then collimated by a 3 m focal length silver mirror and the chirp is compensated using a set of rotatable fused silica flat windows for fine adjustment of the dispersion.

The spectrum is directly monitored using an InGaAs spectrometer and the temporal characterization is performed using dispersion-free third-harmonic generation optical gating (THG-FROG). The evolution of the spectral broadening is shown in Fig. 3. The pressure in the two gas cells is optimized in order to achieve the broadest final spectrum after the two compression stages. This is done by moderately broadening the spectrum in the first stage in order to preserve clean temporal and spatial beam profiles. In this case, the pressure in the first cell is increased to 1 bar.

From 0.6 bar upwards we observe the formation of a distinct second peak in the spectrum near 1850 nm while the broadening tends to slightly blueshift the overall spectrum of the pulse. The main broadening process involved in filamentation is via the Kerr nonlinearity (n_2) induced self-phase modulation. A time-dependent non-linear phase $\phi_{NL} = 2\pi \cdot n_2 \cdot E(t)^2 \cdot L/\lambda_0$ (L is the propagation distance, λ_0 is the carrier wavelength; n_2 is directly proportional to the gas pressure) is indeed accumulated while the pulse propagates, so that new frequencies are produced in the spectrum $\Delta\omega = -\mathrm{d}/\mathrm{d}t(\phi_{NL})$. The time-dependent intensity envelope thus produces red-shifted components near the leading edge of the pulse and blue shifted ones at the trailing edge (assuming an initial smooth bell-shaped pulse). Pure SPM broadening exhibits an oscillatory behavior, the number of peaks being associated with the maximal acquired non-linear phase ϕ_{MAX}. The origin of these peaks is the production of the same chirp within the pulse at different times and their interference. For a symmetric pulse envelope, a SPM broadened pulse should then exhibit symmetric peaks about the central carrier frequency. An additional effect, self-steepening, however breaks this symmetry. As the refractive index $n(t) = n_0 + n_2 I(t)$ is larger in the center of the pulse than on the edges, the trailing part of the pulse propagates faster than the center, inducing a pulse steepening and eventually an optical shock [27]. This temporal asymmetry, in turn, modifies the spectrum as the steepness of the slopes on both edges of the pulse become asymmetric. As a consequence, the intensity of the red-shifted peak is strongly enhanced as compared to the blue-shifted ones. On the other hand, the spectral broadening on the blue side is wider than on the red side [28]. This prominence of the red-shifted SPM peak at 1850 nm, as

Optics EXPRESS

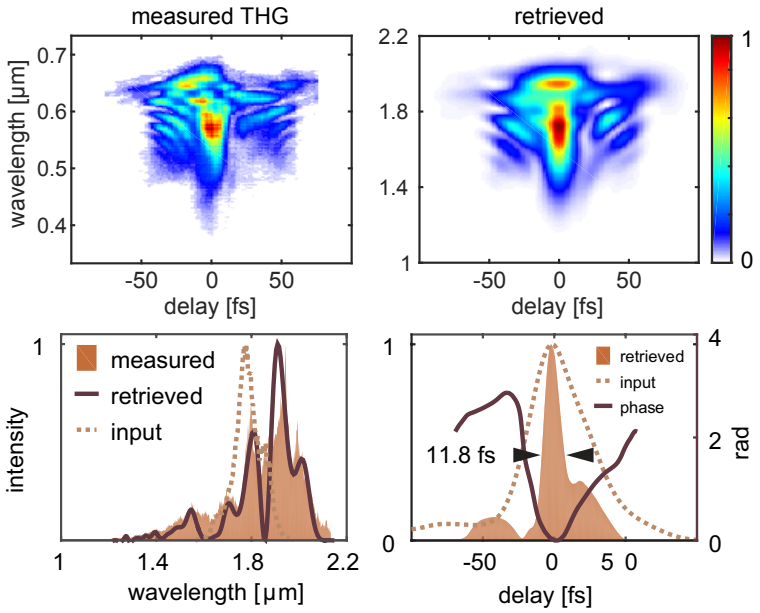

Fig. 4. Frequency-resolved optical gating characterization of the compressed driving pulse. Top: THG FROG measured trace and the multi algorithm retrieved trace. Bottom left: normalized comparison in the spectral domain of the OPA Idler (input), the same pulse after broadening and compression (measured) and the retrieved spectra (retrieved). The input spectrum is centered at 1.79 μm with a 145 nm bandwidth and the measured spectrum shows a main peak shifted at 1.96 μm and is 400 nm wide at FWHM. Bottom right: time domain representation of the retrieved intensities of the OPA pulse (input) and the compressed pulse (retrieved). The retrieved phase (right axis) is given for the compressed pulse only.

well as the broader blue wing, are well observed in Fig. 3, as the pressure increases from 0.6 bar to 1 bar. The filamentation process has been shown to increase this red-shifting, especially in the few-cycle regime [29]. Note that the red-shifting was recently observed both for filamentation in krypton in the same spectral range [9] as well as in spectral broadening in a hollow-core fiber [23]. In particular, the self-steepening process and associated red-shifting appears significant for the recompression by a transparent bulk material [23]. Increasing the filling argon pressure above 1 bar deteriorates the pulse-to-pulse stability and the spatial profile, therefore we limited the pressure in the first cell to this value. The broadened pulse exiting from the first cell was then recompressed in fused silica and refocused by a 2 m focussing mirror in the second argon cell, which pressure was optimized. Again a clear red-shifting of the main peak in parallel to stronger blueshift broadening is observed as soon as the pressure is increased. At 1.3 bar, which corresponded to the highest pressure for stable operation, the spectrum covers the wavelength range from 1200 to more than 2100 nm with a 400 nm FWHM bandwidth and a main peak at 1960 nm.

The temporal characterization of the 1.8 μm pulse is carried out using THG-FROG. The retrieved pulse spectrum is in good agreement with an independently and directly measured spectrum. The retrieved pulse temporal profile shows that the pulses are compressed by a factor of more than 4, down to 11.8 fs as summarized in Fig. 4. With these characteristics, the peak power of the pulse reaches as much as 0.2 TW, and an average power of 2.1 W. The losses in the whole compression process are as low as $\sim$ 15 %, mainly due to Fresnel losses in the cell windows. This also confirms the low plasma density generated in the filaments in our case.

To quantify the energy losses due to the filamentation in the two broadening stages, we measured the mean power at the output of each stage for different pressures of argon. We started with a primary vacuum in both cells and gradually increased the pressure in the first cell up to 2.5 bar. Then we fixed the pressure of the first cell at 1 bar and increased the pressure in the second cell up to 2 bar as shown in Figs. 3(c) and 3(d).

Moreover, the spatial beam profile after the 2-stage filamentation is excellent, as depicted in Fig. 2(b). This feature is characteristic of optimized filamentation schemes, where self-cleaning of the spatial mode occurs [30] mainly due to the spatial dependence of the Kerr induced non-linear refractive index in the incoming beam [31, 32].

4. CEP stabilisation

Transient absorption spectroscopy relies on stable soft-X-ray sources. The stability over the time scale of the measurement is crucial in order to see the minor absorption features as the signal is obtained by comparing the transmitted spectrum with a reference one.

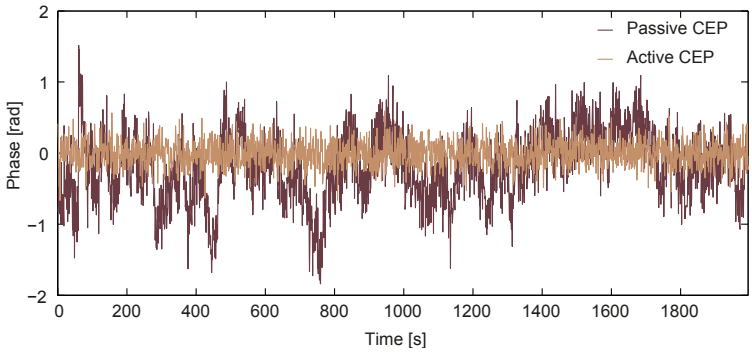

Fig. 5. Carrier envelope phase measured over 30 min using a f-$2f$ interferometry setup. Passive free-running CEP (maple), corresponding to $r.m.s.$ = 531 mrad jitter where the actively locked CEP (brown) stabilization reduce it to $r.m.s.$ = 180 mrad.

In the few-cycle regime the generation of a stable soft-X-ray spectrum depends not only on the intensity stability of the driving source, but also on the CE phase [33] which can be used for the production of isolated attosecond pulses [14, 24].

We employ a passive CEP control scheme [34] for stabilizing the phase of the idler pulses. This is enabled by the white light supercontinuum seeding of the parametric amplifier, where the phase of the idler pulses is passively stabilized due to difference frequency generation between the while light supercontinuum and the pump pulse. The residual phase variation due to drifts in the slightly different optical path lengths of the seed and pump pulses is compensated using a piezo actuator (see Fig. 5). The reflection of the cell output Brewster window is picked up and sent to an f-$2f$ setup for active CEP stabilization.

5. Discussion

Recent spectacular progress has been achieved in the development of table-top soft-X ray attosecond sources covering the whole water window. Typically, HHG in the water window spectral range relies on high-ionization-potential gases such as He and long-wavelength sub-2 cycle driving sources. For time-resolved spectroscopic investigations like soft X-Ray transient absorption, a high flux is necessary, which requires high-peak-power mid-IR sources at high repetition rates. In particular, recent investigations based on post-compression in hollow-core fibers showed that both high flux and cut-off frequencies the oxygen K-edge [35] are achievable.

Optics EXPRESS

As an attractive alternative, here we present the development of a CEP stable sub-2 cycle 0.2 TW mid-IR source at 1 kHz based on filamentation, and associated smooth HHG spectra covering the whole water window including the K-edge of oxygen. Filamentation provides significant advantages, such as negligible losses, spatial mode cleaning, and ease of operation. We intend to use this high-brightness source to investigate peptides and small protein dynamics in solution [4] by transient soft X-ray spectroscopy in the near future.

In this case, the main improvement is the high peak power of the 1.8 μm pulse both available to pump the samples and drive the X-ray generation by HHG with high flux. We demonstrate that filamentation is suitable for efficient pulse compression and generation of clean driving pulses for HHG with minimum power losses.

Appendix

For spectroscopic applications it is common to represent the aborption spectra in optical density and logarithmic scale as shown in Fig. 1. However, for the spectrometer calibration purposes we used carbon K-absorption line at 282 eV best visible in the high-order harmonic spectrum plotted in linear scale as shown in Fig. 6.

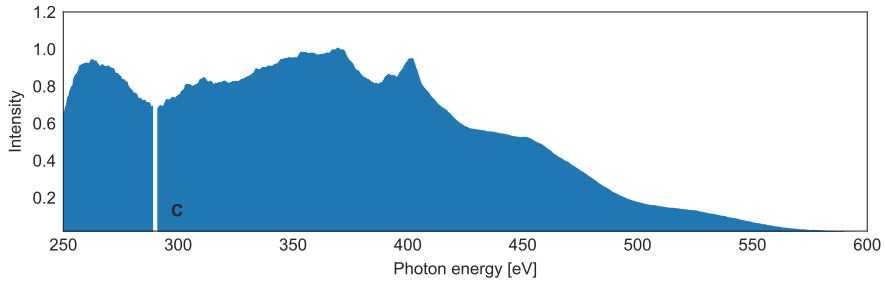

Fig. 6. Typical soft X-ray high harmonic spectrum in linear scale. The white line shows the absorption of the carbon (C) K-edge at 282 eV due to contamination in the beam-line.

Funding

NCCR-MUST, a Swiss National Science Foundation (SNSF) project (200021_159875); ERC Starting Grant (307270-ATTOSCOPE); T.B. acknowledges funding from the EU H2020 research and innovation programme under the Marie Skłodowska-Curie grant agreement No 798176.

Acknowledgments

The authors thank Michel Moret, Fernando Ardana and Luigi Bonacina for technical support.